

Theory of isotope fractionation on faceted ice crystals


Sample manuscript – to show paragraph numbering style and paragraph points.‡

Abstract (Do not number the abstract paragraph or paragraphs.)

Present models of the differential incorporation of isotopic water molecules into vapor-grown ice omit surface processes that may be important in temperature reconstructions. This article introduces a model that includes such surface processes and shows that differences in deposition coefficients for water isotopes can produce isotope fractionation coefficients that significantly differ from those of existing theory. For example, if the deposition coefficient of H_2^{18}O differs by just 5% from that of ordinary water (H_2^{16}O), the resulting fractionation coefficient at 20% supersaturation may deviate from the kinetic fractionation (KF) prediction by up to about $\pm 17\%$. Like the KF model, this “surface-kinetic” fractionation model generally predicts greater deviation from the equilibrium prediction at higher supersaturations; indeed, the sensitivity to supersaturation far exceeds that to temperature. Moreover, the model introduces possible new temperature dependencies from the deposition coefficients. These parameters need to be constrained by new laboratory measurements; nevertheless, the theory suggests that observed $\delta^{18}\text{O}$ changes in ice samples are unlikely to be due solely to temperature changes.

‡ Based on a manuscript by Jon Nelson

1. Introduction



[1] Ever since the late 1950s, the fractionation of isotopes during the vapor deposition of ice has been used to make temperature reconstructions from ice cores (see, e.g., Langway Jr., 2008). In particular, the empirical relation between $\delta^{18}\text{O}$ (or another water isotopologue) in surface snow and the mean surface temperature of a given region has been used to estimate trends in the formation temperatures of ancient ice in cores extracted from the same region (e.g., Dansgaard et al., 1969). However, because a crystal can form at various regions of the atmosphere and grow while falling through layers of variable temperature before reaching the surface, the mean surface temperature may not equal the crystal's condensation temperature. So, how precisely can we determine a crystal's condensation temperature based on its isotope content?

[2] Such condensation temperatures have been estimated from equilibrium fractionation theory. But in 1984, Jouzel and Merlivat, hereafter "JM", showed that this theory disagrees with the empirical surface-snow relation. Their solution was to replace the equilibrium fractionation coefficient with a supersaturation-dependent kinetic fractionation (KF) coefficient. By selecting the right supersaturation-temperature relation, their model could fit the $\delta^{18}\text{O}$ observations. But the KF coefficient ignores surface processes that are crucial to the growth of faceted crystals. If we consider such processes in a new theory, how much might the fractionation coefficient change? And could this change affect temperature reconstructions?

[3] This paper develops a theory of fractionation on faceted crystals that includes surface processes. The resulting fractionation coefficient α differs from the KF prediction by an amount $\Delta\alpha$ that may be as large as $\pm 17\%$. As described in section 5, this $\Delta\alpha$ gives an uncertainty in the inferred (i.e., reconstructed) temperature of 15 °C, though in practice, several factors will lower this uncertainty. But because the surface effect is potentially large, new experiments on α for faceted crystals are greatly needed.

2. Background

2.1 Facetted growth implies regulation by surface processes

[4] The surface of growing atmospheric ice crystals often consists of crystalline facets, sometimes wholly so, which indicates a reduction of growth rate from surface processes (Nelson and Baker, 1996). Without such surface processes, an initially spherical frozen droplet would remain spherical as the crystal grew until being perturbed by a sufficiently large temperature or vapor-density non-uniformity, after which rounded protrusions would develop. Instead, initially spherical frozen droplets quickly grow into a great variety of shapes. Thus, the existence of facets, however small, indicate an influence of surface processes, and if these processes affect the incorporation of ordinary water into ice, they are likely to also affect the incorporation of isotopic water. That is, surface processes should affect isotope fractionation.

2.2 Crystal growth with vapor and surface impedances

[5] The net vapor flux F ($\# \text{ m}^{-2} \text{ s}^{-1}$) of ordinary water molecules to an ice surface is (e.g., Nelson and Baker, 1996)

$$F = \frac{v}{4} \beta (N_S - N_{EQ}) \equiv \frac{v}{4} \beta N_{EQ} \sigma_S, \quad (1)$$

where v is the mean vapor-molecule speed, N_S is the vapor number density at the surface (molecules m^{-3}), N_{EQ} is the equilibrium vapor number density, a function of the surface

temperature T_S , σ_S is the surface supersaturation, and β is the deposition coefficient function. In general, β ranges between 0 and 1, depending on both T_S and σ_S , and depends on whether the crystal face is basal, prism, or some other orientation. Through section 3, we assume all faces are identical and thus described by just one β . In section 4, we consider more realistic crystals with two face types.

[6] The surface supersaturation lies below the far-field supersaturation $\sigma_\infty \equiv (N_\infty - N_{EQ})/N_{EQ}$, where N_∞ is the far-field vapor density, by an amount that depends on how the surface and surroundings impede growth. Specifically,

$$\sigma_s = \frac{\sigma_\infty}{\beta Z}, \quad (2)$$

where Z , a dimensionless number, is the total impedance to growth discussed below (Kuroda, 1984; Yokoyama and Kuroda, 1990; Nelson and Baker, 1996). Here and elsewhere, the same relations also hold for each isotope type, whether HDO (i.e., HD¹⁶O) or H₂¹⁸O, except with different values of the quantities F , ν , N_S , N_{EQ} , β , N_∞ , and Z . These quantities thus have superscript 'i', which stands for either “HDO” or “H₂¹⁸O”.

[7] The total impedance equals the sum of Z_V , the vapor diffusion impedance, Z_H , the thermal impedance, and Z_S , the surface impedance. Z_V accounts for the impedance of the vapor diffusing through air to the crystal surface and increases in proportion to the crystal size times ν/D (Appendix A). Larger crystals are surrounded by larger vapor-depleted regions and thus have greater impedance. As an example, at sea-level pressure, a spherical crystal starting at 1- μm radius and ending at 500 μm has Z_V values increasing from 7.5 to 3700. At lower pressures, Z_V decreases in proportion to the pressure decrease. The thermal impedance arises from the temperature rise of the crystal, the temperature at which the latent heating balances thermal diffusion to the surrounding air. Its magnitude

decreases rapidly with decreasing temperature (in proportion to N_{EQ}) and is less than Z_V below about $-5\text{ }^\circ\text{C}$ (Nelson & Baker, 1996). So to simplify the expressions, we drop Z_H , though it can easily be added to Z_V in all that follows.

[8] The surface impedance equals the inverse of the deposition coefficient:

$$Z_s \equiv \frac{1}{\beta} . \quad (3)$$

This impedance results from an increase in surface-mobile molecules that desorb from the surface. The number of such molecules per area of surface exceeds the equilibrium value because the supersaturated vapor produces a greater-than-equilibrium flux of molecules to the surface and some of the excess molecules do not reach the strong-binding sites on a surface step. Thus, a molecule may fail to reach a step, or having reached a step, fail to bind to the step. On a micron-or-larger facet, the fraction of the incident molecules that reach a step should be significantly below unity.

3 Basic theory of surface-kinetic fractionation

[9] Under constant conditions, the ratio χ of the number of isotope molecules to H_2O molecules in the crystal equals the ratio of their respective net vapor fluxes to the surface. From eqs. 1 and 2, this ratio equals

$$\chi = \frac{(N_\infty^i - N_{EQ}^i) (1+z)}{N_{EQ} \sigma_\infty d' (1+z^i)} , \quad (4)$$

where $z \equiv Z_S/Z_V$ and $d' \equiv D/D^i$, the ratio of the vapor diffusion constants. But, by definition of the equilibrium fractionation coefficient α_S (JM, eq. 7), the corresponding isotopic number ratio in the vapor differs from that in the solid by the equilibrium fractionation ratio for ice:

$$\frac{N_{EQ}^i}{N_{EQ}} = \frac{\chi}{\alpha_S} . \quad (5)$$

(Formulas in Jouzel (1986) for α_S are $\ln \alpha_S = 11.839/T - 28.224 \times 10^{-3}$ for $H_2^{18}O$ and $\ln \alpha_S = 16288/T^2 - 9.34 \times 10^{-2}$ for HDO.) We define the nonequilibrium fractionation coefficient α like that in eq. 5 except with the far-field, non-equilibrium, vapor density:

$$\frac{N_{\infty}^i}{N_{\infty}} = \frac{\chi}{\alpha} . \quad (6)$$

Using eqs. 4, 5, and 6 to eliminate N_{EQ}^i , N_{∞}^i , and χ , one gets

$$\alpha = \frac{1 + \sigma_{\infty}}{\frac{1}{\alpha_S} + \sigma_{\infty} d' \frac{1 + z^i}{1 + z}} . \quad (7)$$

[10] Three limits of eq. 7 stand out: the equilibrium limit, the KF limit, and the surface-kinetic limit. In the first, $\alpha \rightarrow \alpha_S$ when $\sigma_\infty \rightarrow 0$. In the KF limit, the surface impedances vanish ($z, z^i \rightarrow 0$) giving

$$\alpha_{KF} = \frac{1 + \sigma_\infty}{\frac{1}{\alpha_S} + \sigma_\infty d'}, \quad (8)$$

which shows that KF fractionation occurs whenever $d' \neq 1/\alpha_S$. Equation 8 agrees with JM's result, though they wrote the equivalent expression as $\alpha_K \cdot \alpha_S$. (Fisher (1991) does a more detailed analysis of the temperature difference between crystal and air, but the result is nearly indistinguishable from the KF result.) Finally, in the surface-kinetic limit ($z, z^i \gg 1$)

$$\alpha_{SK} = \frac{1 + \sigma_\infty}{\frac{1}{\alpha_S} + \sigma_\infty yx}, \quad (10)$$

showing that surface fractionation occurs when $yx \neq 1/\alpha_S$.

[11] Thus, fractionation depends on four factors: α_S , d' , y , and x . Physically, α_S arises from different isotopic rates of desorption of an equilibrium distribution of water species on the ice surface. But under supersaturated conditions, vapor flows to the ice surface, producing additional fractionation due to different isotopic rates of vapor diffusion (d'), molecular impingement to the surface (y), and desorption from the surface (x). The isotopic desorption rates change because the surface has a greater-than-equilibrium

concentration of mobile water species; the species with a lower deposition coefficient will have a greater increase in mobile molecules on the surface, and thus a corresponding increase in desorption rate. The first three factors are close to unity (Table 1) and independent of supersaturation. However, x may vary with supersaturation and is presently unknown. Here, we assume a range of $0.8 \leq x \leq 1.2$ as described in Appendix B.

[12] For surface fractionation to be significant, the surface impedance must be comparable to, or larger than, the vapor impedance. To determine the surface impedance, we must estimate β and β^i for a given set of conditions. These conditions influence β through σ_s . We can approximate various functional forms using two parameters σ_1 and n as

$$\beta = \left(\frac{\sigma_s}{\sigma_1} \right)^n, \quad (10)$$

where $n > 0$ and σ_1 is a characteristic supersaturation that depends on temperature and surface properties of the crystal facet. To determine β and σ_s , one must combine eq. 10 with eqs. 2 and 3. In the linear and quadratic cases ($n = 1$ or 2), one can solve for β analytically and deduce σ_s , but the general case requires a numerical method. Numerical results are described in Appendix C and used in the calculations for Figs. 1 and 2.

[13] At a given temperature and supersaturation, two variable factors affect α : the surface impedance ratio z for regular water and the ratio of surface impedances $x \equiv \beta/\beta^i$. The former increases with an increase in either the parameter σ_1 or n , but decreases with increasing crystal size, as shown in Fig. 1. In addition, z increases with elevation due to the air-pressure dependence of D .

[14] Deviations from the KF prediction occur at large z and when x differs from the KF limit of d' . When $x < 1$, the deposition coefficient of the isotope exceeds that of regular water, making the ice richer in isotope by an amount that depends on z . For example, at relatively high surface impedance, as in the upper ‘beaded’ curve in Fig. 2 ($z > 3$ over the entire supersaturation range), the fractionation lies above the KF value because $x = 0.95$, which is less than $d' = 1.03$. But, as x is not below $1/\alpha_S$, the fractionation does not exceed the equilibrium value, instead lying roughly halfway between the KF and equilibrium values. Similarly, when $x > d'$, the surface fractionation acts in the same direction as KF, driving the degree of fractionation even lower. For example, when x is instead 1.05, the fractionation lies distinctly below the KF curve (Fig. 2, lower beaded curve). In this case, the fractionation from y acts together with that from x , increasing the effect.

[15] If x deviates further from unity, the surface impedance need not be large for surface fractionation to have a large effect. For example, with middling values of z , the fractionation exceeds α_S when $x = 0.8$ (Fig. 2, top curve). And when $x = 1.2$, the surface fractionation may lie below the KF value by an amount nearly double the amount KF lies below the equilibrium value (Fig. 2, bottom curve). In contrast, at low surface impedance, the fractionation remains close to the KF value even when the x value deviates 20% from unity.

4 Surface-kinetic fractionation to realistic crystals

4.1 Cylindrical crystals

[16] We now make the model more realistic by considering crystals shaped as tabular or columnar cylinders. In addition to introducing the variable height/width ratio (aspect

ratio), the cylinder case has two distinct faces, with the top/bottom, or “basal” face having fractionation value α_B , and the side or “prism” face having value α_P .

[17] These fractionation values follow from eq. 7 with the appropriate substitution; for example, for α_B , we substitute z_B for z and z_B^i for z^i . Concerning z_B and z_P , the surface impedances equal the reciprocals of β_B and β_P , just as in the sphere case, but the vapor impedances are more complex, depending not only on crystal size, but also on shape and rate of shape change (see Appendix A).

[18] To determine values for $\alpha_{B,P}$, one must know the deposition coefficients, which means determining just one number: σ_S . With a nonspherical crystal such as the cylinder, σ_S varies along the surface. But, as described elsewhere (e.g., Wood et al., 2001), the point of highest σ_S determines the growth rate and thus is the appropriate σ_S value for the deposition coefficient (eq. 10). This point is usually the edge of the facet (unless some face has essentially stopped growing (Nelson, 2001)). Here, we assume this is the case for both the basal and prism facets. As a result, the σ_S value solves

$$\sigma_S = \frac{\sigma_\infty}{1 + \beta_B(\sigma_S)Z_{VB}} = \frac{\sigma_\infty}{1 + \beta_P(\sigma_S)Z_{VP}}, \quad (11)$$

which is similar to eq. 2.

[19] To get the mass-averaged α , one multiplies each coefficient by the mass-uptake (flux times facet area) on the corresponding facets:

$$\alpha = \alpha_B \frac{\gamma}{\gamma + 2\Gamma} + \alpha_P \frac{2\Gamma}{\gamma + 2\Gamma}, \quad (12)$$

where $\gamma \equiv \beta_B/\beta_P$ is the growth-rate ratio (Nelson and Baker, 1997). For example, in steady-state, $\gamma = \Gamma$, and thus 2/3 of the mass enters via the prism faces. But in general, a range of fractionation values can occur, depending on the crystal aspect ratio, the growth-rate ratio, and the fractionation to each face. The last factor depends on the ratios of the deposition coefficient functions $x_B \equiv \beta_B/\beta_B^i$ and $x_P \equiv \beta_P/\beta_P^i$.

[20] Results show that the crystal shape affects fractionation at high z , particularly when the deposition coefficient ratios differ between the faces. For example, when $z > 2.5$ (all solid curves in Fig. 3), but both facets have the same x ratio of 1.05, the fractionation coefficient is only slightly less than the sphere result. This is shown by curve 1 in which $\Gamma = \gamma = 10$. At larger Γ , the fractionation coefficient decreases further, though the effect remains relatively small. Larger influences on α can occur when $x_B \neq x_P$. In particular, for steady-state growth ($\gamma = \Gamma$) with $\Gamma = 10$, fractionation decreases when $x_P > x_B$ (curve 2), even though their average still equals 1.05 because in steady state most mass enters through the prism face, which has an x_P value of 1.1.

[21] Usually Γ deviates further and further from unity during growth (Takahashi et al. 1991), meaning $\gamma \geq \Gamma$ for columns and $\gamma \leq \Gamma$ for plates. In the non-steady-state case of curve 3, most mass enters through the basal face, and in this case $x_B = 1.1$, bringing the curve lower. Similarly, when nearly all of the mass enters through the prism face, as in the tabular-crystal case in curve 4, then the fractionation coefficient is significantly below that of the sphere when $x_P = 1.1$. These cases (2-4) show deviations in α below that of an equivalent sphere of $x = 1.05$ because the face with most of the mass uptake had $x = 1.10$. If instead they had $x = 1.00$, then the resulting α value would be above that of a sphere. These cylinder results emphasize what we found with the sphere: when the surface impedance dominates, small changes in x can introduce relatively large variations in

fractionation coefficient. For the cylinder, this applies to small changes in x on the facets that dominate growth.

4.2 Incompletely faceted crystals

[22] Stellar and hollowed crystals are incompletely faceted, meaning that some of the mass uptake comes from non-faceted (NF) regions. For this case, we need an extra term in eq. 12:

$$\alpha = \alpha_B M_B + \alpha_P M_P + \alpha_{NF} M_{NF}, \quad (13)$$

where M_j stands for the fraction of mass uptake that occurs through face type “j” and α_{NF} equals the fractionation coefficient for non-faceted regions. The latter coefficient should equal α when $\beta \rightarrow 1$, and thus nearly equal α_{KF} .

[23] For stellar or dendritic crystals, it is hard to accurately estimate M_P and M_{NF} without newer, more careful measurements. I attempted such an estimate in Nelson (2005), using the measurements of Takahashi et al. (1991), and found that M_{NF} varied between 0.77 and 0.87 for crystals between -13.3 and -16.8 °C. Thus, most of the mass uptake on such crystals occurs on the non-facet regions.

[24] A similar difficulty occurs with hollowed columns, except the problem instead lies in estimating M_B and M_{NF} . However, if we assume that the hollowed regions are cylindrical cones extending to the crystal center, and if the volume of the hollows remain a fixed fraction K of the volume of the equivalent non-hollowed crystal, then the resulting mass-uptake fractions can be shown to equal

$$M_B = \frac{\gamma}{\gamma+2\Gamma} \frac{1-3K}{1-K}, \quad M_P = \frac{2\Gamma}{\gamma+2\Gamma} \frac{1}{1-K}, \quad M_{NF} = \frac{2K}{\gamma+2\Gamma} \frac{\gamma-\Gamma}{1-K}. \quad (14)$$

When the hollow extends across the entire basal face, K has its maximum value of $1/3$. In this case, $M_B = 0$ and the fraction of mass uptake by the non-facet region M_{NF} has its maximum value, a value that depends on γ/Γ . Using the measurements for hollow columns at -5.3 °C from Takahashi et al. 1991, $\gamma/\Gamma = 5.4$, giving $M_{NF} = 0.6$. As the hollows did not appear to extend across the basal faces, this value may be an overestimate. Nevertheless, significant amounts of uptake likely occur in the non-facet regions of hollow columns.

5 Discussion: The need for new measurements

[25] In many regions, precipitating ice largely consists largely of single-crystalline and aggregates of incompletely faceted forms, forms for which the existing KF model may suffice because of the large uptake on non-faceted regions. However, precipitating crystals in polar regions (e.g., Lawson et al. 2006), crystals in cirrus and other high clouds, as well as surface hoar often consist of mainly faceted forms for which the new surface-kinetic model may be required.

[26] To estimate how the present uncertainty in α for faceted crystals could produce uncertainty in inferred temperature T' of precipitated ice, we transform the uncertainty in α to the uncertainty in the relative deviation of isotopic content in ice δ_c , and then this uncertainty to a temperature uncertainty. In our notation

$$\delta_c = \frac{\chi - \chi_{SMOW}}{\chi_{SMOW}} = \alpha \frac{N_\infty^i / N_\infty}{\chi_{SMOW}} - 1, \quad (15)$$

and thus an uncertainty in α of $\Delta\alpha$ gives an uncertainty in δ_c of

$$\Delta\delta_c = \Delta\alpha \frac{N_\infty^i / N_\infty}{\chi_{SMOW}} \approx \Delta\alpha. \quad (16)$$

Using the modeled gradient of ^{18}O with respect to the condensation temperature $d\delta_c^{18}\text{O}/dT_c$ from Jouzel et al. (1997), the uncertainty in inferred temperature T' of precipitated ice is approximately

$$\Delta T' \approx \frac{\Delta\delta_c}{d\delta_c^{18}\text{O}/dT_c} \approx \frac{\Delta\alpha}{1.1\text{‰}/^\circ\text{C}}. \quad (17)$$

Thus, equating the possible range in α from Fig. 2 ($\sim\pm 17\text{‰}$) to the uncertainty $\Delta\alpha$, the uncertainty in the inferred crystal growth temperature equals about 15°C , a large value. However, the uncertainty in the inferred paleoclimatic temperatures would probably be much less, reflecting a convolution of $\Delta\alpha$ with the relative changes in supersaturation and degree of crystal faceting during a past climate shift. The effect of surface-kinetic fractionation may also be lessened because the ice record in a given layer is the yearly accumulation, and thus will have a greater mass contribution per crystal from the larger crystals that have less uptake on facets.

[27] Nevertheless, the surface effect, large or small is unknown. Previous vapor-to-ice fractionation experiments are limited to largely non-faceted crystals. Specifically, Jouzel and Merlivat (1984) exposed a $-20\text{ }^{\circ}\text{C}$ surface to water vapor at $20\text{ }^{\circ}\text{C}$, conditions that produce highly dendritic frost crystal forms. Uemura et al. (2005) analyzed similarly dendritic frost forms. Thus, although those experiments were appropriate for testing the KF model, they cannot be used to understand surface fractionation. Instead, to test this model, we need new experiments on completely faceted crystals.

[28] Moreover, because α depends on both T and σ_s , if we measure the dependence for both HDO and H_2^{18}O , one could then, in principle, use observed $\delta^{18}\text{O}$ and δD values to infer both the deposition temperature and supersaturation of an ice sample.

6 Conclusions

[29] Unlike kinetic fractionation theory, the surface-kinetic theory includes potentially important surface processes on faceted ice crystals. When the surface impedance to growth is low, both the kinetic and surface-kinetic models give similar predictions, showing significant deviations to equilibrium fractionation at moderate-to-high supersaturations. In contrast, when the surface impedance is comparable to the vapor impedance, the fractionation coefficient depends sensitively on the ratio of the deposition coefficient functions of the ordinary and isotopic water molecules, giving results that deviate sharply from kinetic fractionation results. Such conditions should hold during the growth of faceted crystals, and since faceted crystals are common in the atmosphere, the new theory should apply to some cases in which the kinetic and the equilibrium theory have previously been used. However, before the new theory can be applied to the atmosphere, we need to either measure the effect directly or experimentally determine the relevant deposition coefficient functions over a range of temperatures and supersaturations.

Appendix A: The vapor impedances

[30] The vapor impedance depends on the crystal shape. For a spherical crystal

$$Z_v \equiv \frac{rV}{4D} , \quad (18)$$

where r is the radius of the crystal. For a cylindrical crystal

$$Z_{VB} = r_B h_{BE} + r_P h_{PE} \frac{\beta_P}{\beta_B} \quad (19a)$$

and

$$Z_{VP} = r_B h_{BE} \frac{\beta_B}{\beta_P} + r_P h_{PE} , \quad (19b)$$

where r_B , r_P , h_{BE} , h_{PE} are from Nelson, 2001, with slight changes that are described next. Here $r_B = Z_v(2/3\Gamma)^{1/3}/2^{1/2}$ and $r_P = Z_v(2/3\Gamma)^{1/3} \Gamma^{1/2}$ are normalized sizes of the top & bottom (basal) and side (prism) faces, with Γ the column length divided by its diameter. Physically, r_B is the radius of the sphere that would have the same area as the basal faces of the cylinder, scaled by the distance $4D/v$ and written in terms of Z_v for the sphere that would have the same volume. This makes it easier to compare to the spherical case. Similarly, r_P is the scaled radius of the sphere with the same area as the prism faces of the cylinder. The two h functions fit

$$h_{BE}(\Gamma) = \sqrt{2} \cdot 10^{-0.1315 \operatorname{Tanh}[0.8060 \{\operatorname{Log}(\Gamma) + 0.1854\} - 0.0639 \operatorname{Log}^2(\Gamma)] - 0.3314} \quad (20a)$$

and

$$h_{PE}(\Gamma) = 0.6902 \cdot \Gamma^{-0.5 + 1/[1.932 + 0.4976 \operatorname{Log}(\Gamma) + 0.1058 \operatorname{Log}^2(\Gamma)]} \quad (20b)$$

(In Nelson, 2001, the values are half the above, but the product rh is the same). Wood et al. (2001) showed that the above basis functions h are very nearly the same as the corresponding basis functions for a hexagonal column of the same aspect ratio.

Appendix B: Estimated range of x

[31] To estimate x , equate β/β^i to the ratio of surface migration distances (see e.g., Yokoyama and Kuroda, 1990). Measurements of the migration distance of ordinary water on ice (Mason, Bryant, and van den Huevel, 1963) indicated that it varied rapidly with temperature, decreasing by a factor of five when temperature decreased from -2 to -6 °C, and then increasing again by the same factor from -6 to -12 °C. If the corresponding curve for the isotope on regular ice is similar in shape, but shifted to higher temperature by a degree or more, β/β^i could be as small as 0.2 or as large as 5.0. Such large deviations from unity, however, may be unlikely, so the plots shown here use ratios between 0.8 and 1.2. Such a range is also consistent with measurements of bulk diffusion constants of HDO and H₂¹⁸O into ordinary ice given that a) the migration distance is proportional to the square-root of the diffusion constant and b) the square-root of the measured ratio of diffusion constants for these two species at 163 K equals 1.3 (Livingston et al, 1997). Although bulk and surface diffusion differ, the measurement shows that two water species can behave differently when diffusing in ice.

Appendix C: Analytic fit for surface impedance

[32] By using a numerical method to solve for Z_S for a range of n , σ_∞/σ_1 , and Z_V , and then fitting the curves to an analytic function, I found an approximate formula for β . The formula estimates z within a few percent of the correct value, for the range of possible values of n , σ_∞/σ_1 , and Z_V . Specifically, if we use the derived parameter

$$\Phi \equiv \left(\frac{\sigma_\infty}{\sigma_1}\right) Z_V^{\frac{1}{n}}, \quad (21)$$

then the resulting fitted function is

$$\frac{Z_S}{Z_V} \equiv Z'(\Phi, n) = 1.5n - z \frac{\Phi^{-(n/(n+1)-1/4)}}{\text{Log}_{10}(1+1.5n\Phi^{-(n^2/(n+1)+1/4})}. \quad (22)$$

These two equations show that when $\sigma_1 > \sigma_\infty$ and n is large, $z \rightarrow (\sigma_\infty/\sigma_1)^{-n} Z_V^{-1}$, which becomes large. In contrast, z decreases as σ_∞ increases. Figure 1 shows both of these trends. Moreover, as Z_V increases during growth, z will decrease during growth.

Acknowledgements

I thank Profs. Marcia Baker and Brian Swanson for their critical reading of the manuscript.

References

Burton, W. K., Cabrera, N., and Frank, F. C.: The growth of crystals and the equilibrium structure of their surfaces, *Phil. Trans. Royal Soc. (London)* A243, 299-358, 1951.

Fisher, D. A.: Remarks on the deuterium excess in precipitation in cold regions, *Tellus* 43B, 401-407, 1991.

Jouzel, J. and Merlivat, L.: Deuterium and Oxygen 18 in Precipitation: Modeling of the Isotopic Effects During Snow Formation, *J. Geophys. Res.*, 89, 11749-11757, 1984.

Jouzel, J.: Isotopes in Cloud Physics: Multiphase and Multistage Condensation Processes, *Handbook of Environmental Isotope Geochemistry*, Vol. 2. The Terrestrial Environment, 61-112, B. P. Fritz and J. Ch. Foutès, Eds., Elsevier, 1986.

Jouzel, J., Alley, R. B., Cuffey, K. M., Dansgaard, W., Grootes, P., Hoffmann, G., Johnsen, S. J., Koster, R. D., Peel, D., Shuman, C. A., Stievenard, M., Stuiver, M., and White, J.: Validity of the temperature reconstruction from water isotopes in ice cores, *J. Geophys. Res.* 102 (C12), 26,471-26,487, 1997.

Kuroda, T.: Rate Determining Processes of Growth of Ice Crystals from the Vapour Phase. Part I: Theoretical Consideration, *J. Meteorol. Soc. Japan* 62, 552-561, 1984.

Lawson, R. P., Baker, B. A., Zmarzly, P., O'Connor, D., Mo, Q., Gayet, J-F., and Shcherbakov, V.: Microphysical and Optical Properties of Atmospheric Ice Crystals at South Pole Station, *J. Appl. Meteor. Clim.*, 45, 1505-1524, 2006.

Livingston, F. E., Whipple, G. C., and George, S. M.: Diffusion of HDO into Single-Crystal H_2^{16}O Ice Multilayers: Comparison with H_2^{18}O , *J. Phys. Chem. B*, 101, 6127-6131, 1997.

Nelson, J.: Growth mechanisms to explain the primary and secondary habits of snow crystals, *Phil. Mag. A*, 81, 2337-2373, 2001.

Nelson, J.: Branch Growth and Sidebranching in Snow Crystals, *Crystal Growth & Design*, 5, 1509-1525, 2005.

Nelson, J. and Baker, M. B.: A New Theoretical Framework for Studies of Vapor Growth and Sublimation of Small Ice Crystals in the Atmosphere, *J. Geophys. Res.* 101, 7033-7047, 1996.

Mason, B. J., Bryant, G. W., and van den Huevel, A. P.: The growth habits and surface structure of ice crystals, *Phil. Mag.*, 8, 505-526, 1963.

Takahashi, T. Endoh, T., Wakahama, G., and Fukuta, N.: Vapor diffusional growth of free-falling snow crystals between -3 and -23 °C, *J. Meteorol. Soc. Jpn.*, 69, 15-30, 1991.

Uemura, R., Matsui, Y., Yoshida, N., Abe, O., and Mochizuki, S.: Isotopic fractionation of water during snow formation: Experimental evidence of kinetic effect, *Polar Meteorol. Glaciol.*, 19, 1-14, 2005.

Wood, S. E., Baker, M. B., and Calhoun, D.: New model for the vapor growth of hexagonal ice crystals in the atmosphere, *J. Geophys. Res.*, 106 (D5), 4845-4870, 2001.

Yokoyama, E. and Kuroda, T.: Pattern formation in growth of snow crystals occurring in the surface kinetic process and the diffusion process, *Phys. Rev. A*, 41, 2038-2049, 1990.

